Extraction of the Equivalent Coupling Surface of a capacitor mounted on a PCB using Near-Field Scan

Wanyoike Dennis, Alexandre Boyer, Serpaud Sébastien

Extraction of the Equivalent Coupling Surface of a capacitor mounted on a PCB using Near-Field Scan

D. Wanyoike[#$*1], A. Boyer [$*2], S. Serpaud[#3]

[#]IRT Saint Exupéry – Toulouse, France
[$]LAAS CNRS – Toulouse, France
*INSA – Toulouse, France

[1]dennis.kamau@irt-saintexupery.com, [2]alexandre.boyer@laas.fr, [3]sebastien.serpaud@irt-saintexupery.com

***Abstract* — This paper presents an approach to extract the equivalent coupling surface of a capacitor mounted on a PCB. This is the first step of developing a methodology to extract the insertion loss of an EMI filter in situ. The approach utilizes near-field scan technique based on H-field probe coupled to a capacitor on a PCB. The value of mutual inductance between the probe and capacitor is then extracted by post processing. Finally, the equivalent coupling surface is extracted by optimization using GEMSEO tools.**

***Keywords* — Insertion loss, Mutual coupling, Power converters, Equivalent coupling surface, Near-field scan.**

I. INTRODUCTION

Power converter modules e.g. SMPS constitute a major source of electromagnetic (EM) emission in electronics. To mitigate the conducted emissions (CE) from SMPS, EMI filters have for a long time been used to attenuate both Differential mode (DM) and common mode (CM) emissions. The noise source and load impedances have an impact on an EMI filter performance in addition to the filter itself. Present-day techniques for evaluating EMI filters, such MIL-STD-220 and CISPR 17 [1], employ standalone filters with fixed source and load impedances (50Ω/50Ω or worst-case analysis). Currently there is the revival of the IEEE 1560 [2], which takes into account non-loaded and loaded attenuation measurements within the range of 100 Hz to 10 GHz, taking into account varying source and load impedances. Additionally, hybrid filtering solutions [3] are becoming widely applied in the industrial context as they are more compact compared to passive solutions. The existing methods of EMI filter characterization cannot be employed to characterize the hybrid filtering solutions. Therefore, there is a need to develop a new approach to characterize EMI filters in the real operating conditions and taking into account the noise and load impedances while also being suitable for application in the hybrid filtering solutions.

As near-field scanning (NFS) technology advances, near-field measurements have gained popularity as a technique for analyzing complicated EMI issue. However, this analysis remains only qualitative (a direct estimation of CE is not possible) and the identification of a hot spot does not indicate necessarily where and how a design correction has to be brought [4]. Research in [5] developed a method to estimate currents flowing within traces hidden within a PCB using NFS results. Another approach is measuring high-frequency currents and voltages is using near-field scans [6-7]. An NFS-based technique has been put out by the authors in [8] to measure how decoupling capacitors affect the power integrity of an unpowered PCB. The proposed method has two main benefits: first, it offers an in-situ, contactless assessment of the attenuation and secondly, it can be used to evaluate both powered and unpowered converters modules, allowing for evaluation of high voltage power converter modules without the risk of damage. This approach is further used in [4] to present and validate an original contactless NFS-based method to quantify the performance of EMI filter mounted on power converter applications. The methodology heavily relies on coupling between a near field H-probe and a component on the PCB. Therefore, a careful extraction of the mutual coupling (*M*) between a near field probe and the component on the PCB is necessary. In [4], this extraction of *M* was carefully done for limited cases of capacitors (3 cases). In this paper, we intend to ensure that we can precisely extract the value of *M* between a probe and a component. Known geometries are first considered (circular loops) and the value of *M* extracted for different geometrical configurations. This is obtained using analytical equations, FEM-CST full-wave simulation and experimental methods and a comparison is made. Using the results of *M* obtained here, the equivalent component coupling surface can be approximated into an equivalent loop of specific geometry, of specific location and orientation, coupling with the near field probe. As a secondary objective, we intend to show that the equivalent coupling surface between a component can be extracted at any point as compared to [9] where it was evaluated only for distinct positions as a TEM cell was used. This paper is organized as follows: Section II describes briefly the principles of the approach. Section III presents the validation cases of *M* extraction and the overall approach is validated in Section IV. Section V validates optimization approach and evaluates the robustness of this approach to noise. This is a crucial step as the experimental data is subject to various noise sources.

II. PRINCIPLES OF THE APPROACH

A. General application of the concept

The methodology to extract the IL of the EMI filter has been introduced in [10] and is described in Fig. 1.

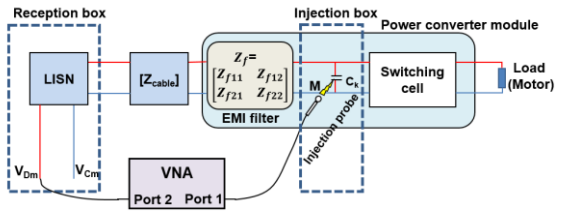

Fig. 1: Extraction of the insertion loss of EMI filter in situ and in a contactless manner [10]

All the filter components between the injection box and the reception box are modelled in to two-port network, and by the evaluation of the S- parameters between these two points, it is possible to extract the IL of the EMI filter as shown in the following equations [10].

$$Z_{12_f} = \pm j\omega \boldsymbol{M} \frac{Z_{21Probe}}{Z_k(Z_{11Probe}+Z_{Lp})} \cdot K_S \cdot \frac{Z_{in_{Filter}}}{Z_{in_{Filter}}+Z_{out_{Cable}}} \quad (1)$$

Where K_S is a term that relates to the test set up impedance.

Finally, IL can be obtained from (2). Both equations show that the evaluation of IL relies on a precise knowledge of the mutual inductance between the H-field probe and the component on which it is coupled.

$$IL(dB) = \frac{\left(Z_{in_{CV}}+Z_{22_f}\right)\left(Z_{out_{Cable}}+Z_{11_f}\right)-Z_{12_f}\cdot Z_{21_f}}{Z_{12_f}\cdot\left(Z_{out_{cable}}+Z_{in_{CV}}\right)} \quad (2)$$

B. *Model of the extraction of M between two loops*

In order to extract the coupling between a circular NFS probe and a component in the PCB, the component e.g a capacitor is to be approximated into an equivalent loop of any shape (e.g. circular or rectangular). In Fig. 2, a primary loop and a secondary loop have been drawn. They have been drawn as perfect circles only for illustration purpose.

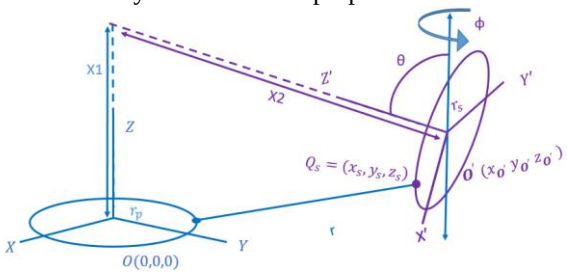

Fig. 2: Illustration of the extraction of coupling between two loops arbitrarily oriented in space (circular geometries chosen for illustration)

The primary loop is located at the origin whose center is $O(0,0,0)$ and on the plane XY along the Z axis. The secondary loop is centered at the point $\boldsymbol{O'}$ $(x_{O'}\ y_{O'}\ z_{O'})$. In order to simplify the approach, the method of the magnetic vector potential $\vec{A}$ is used to extract the mutual coupling between the two loops, whatever their geometry and respective orientations. The magnetic vector potential $\vec{A}$ at point on the secondary loop $Q_s = (x_s, y_s, z_s)$ produced by the differential element $d\vec{l}_P$ on primary loop carrying the current I_{pr} is given by (3).

$$\vec{A}_\varphi = \frac{\mu_0}{4\pi}\int_{l_P} \frac{I_{Pr}}{r} d\vec{l}_P \quad (3)$$

Using Stokes theorem, the mutual inductance is computed from the magnetic flux by (4).

$$M = \frac{\Phi_s}{I_{Pr}} = \frac{\mu_0}{4\pi} \oint\oint \frac{d\vec{l}_P\ d\vec{\ell}_S}{I_{Pr}} \quad (4)$$

This integral has been solved in [11]. With the knowledge of the secondary and the primary loops parameters, locations, and their orientation to each other, this equation is implemented using a python code and the value of *M* between the two loops evaluated at different positions of the loops. An assumption that is made in the implementation of this code is that, the cross-section is negligibly small compared to the separation distance and the current is concentrated on the outer surface of the loop. In order to compare the results obtained using this coding method, full-wave simulation based on CST software (FEM solver) is done replicating the coded parameters and the results are compared. In our approach, the final application is in power converters. Thus, regarding the separation distance and the frequency, the impact of retarded potential can be ignored and does not impact the value of *M*.

C. *Extraction of the equivalent coupling surface of a capacitor*

Fig. 3 presents the flowchart used to extract the equivalent coupling surface (ECS) of a component from NFS measurements.

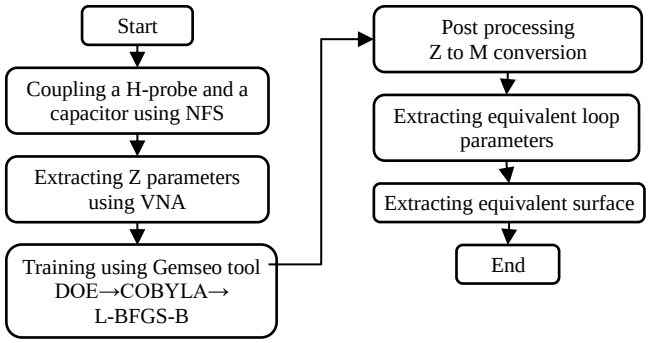

Fig. 3: Flowchart showing the approach to extract the Equivalent coupling surface of EMI filter components.

By experimental measurements, *M* between a H-field probe and an EMI filter component is evaluated and this data is used to create a dataset. The H-field probe is moved at different positions around the component on a PCB. Both the H-field probe and the component are connected to the VNA ports. The connection from the component to the SMA is made using a very short trace. Using the VNA, the Z_{21} parameters are measured and the value of *M* is obtained according to (5). An optimization model provided in GEMSEO tools [11] is fed with this dataset in order to predict the unknown parameters of the ECS of the EMI filter component, in this case a capacitor.

$$Z_{12}^{pc} = jM\omega, \Rightarrow M = \frac{Im\,(Z_{12}^{pc})}{\omega} \quad (5)$$

The GEMSEO optimization method adopted is a two-step optimization method. First, Design of Experiments (DOE) is used to investigate feasible basins in general. Here, a Latin Hypercube Sampling (LHS) of the 5-D parameter space (R_P, x, y, z, θ) is used. The COBYLA solver, which robustly manages bounds and linear constraints, is then used to refine the best DOE sample. The COBYLA solution is then high-precision refined using a gradient-based L-BFGS-B minimization.

Finally, a systematic multistart L-BFGS-B is used. LHS is used to get five initial guesses that are widely distributed. Then an L-BFGS-B is run starting from each seed, until it converges, after which the closest result, the one with the lowest error, is chosen. The DOE and COBYLA are derivative free, while multistart L-BFGS-B requires gradient which is estimated by L-BFGS using finite differences.

III. Validation of the Extraction of *M*

In this section, the *M* values computed by our code are compared to full-wave simulation and experimental measurements for validation purpose. Circular geometries are considered, with various loop locations, orientations and dimensions. Three loops, with diameters of 9.5, 6.5 and 8 mm, are designed at the end of a semi-rigid coaxial cable, whose wire is 0.5 mm thick. In simulation, perfect circles are considered, contrary to the home-made loops. The simulation models are illustrated in Fig 4. Perfect electrical conductor is considered as material.

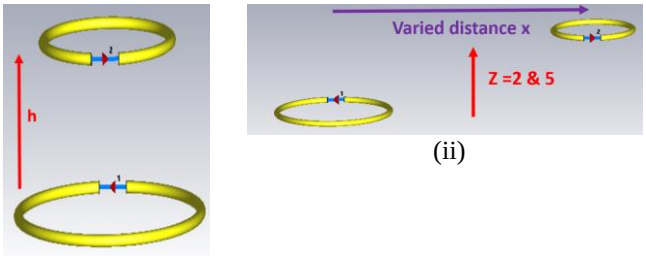

(i) (ii)

Fig. 4: Loops design in FEM-CST Full-wave simulation (i) Coaxial positions (ii) Parallel axis positions

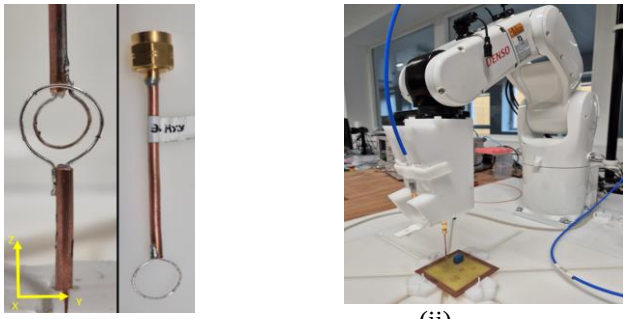

(i) (ii)

Fig. 5: Two probes, 9.5 and 6.5 mm arranges in a coaxial position. Next is a picture of a 9.5 mm probe. (ii) The NFS robot station

Two orientations are evaluated: coaxial positions (loops centers are held in coaxial positions and the distance of separation varied Fig 4(i)), parallel axis positions (where the planes of the loops are parallel Fig 4(ii)) are analyzed. Frequency domain solver is used and tetrahedron meshing is done. The third method of extracting *M* is done experimentally. Circular H-probes of diameters 9.5 mm, 6.5 mm and 8 mm are connected using a (50 Ω) SMA and coaxial to the VNA. One probe is held at a constant position while the other probe is moved (Fig 5 (i)). A calibration of the VNA using RS-ZV-Z135 calibration kit is done at the 60 mm point from the loops. A bandwidth of 10 kHz is used and a frequency range of 100 kHz to 1 GHz is configured. The probe connected to the NFS robot is then moved, Fig 5 (ii) and the value of *M* is extracted as in (5).

Below is a comparison of the results of *M* obtained using the three methods. As seen in Fig. 6, there exists a high correlation between *M* for each of the three methods. An average Pearson correlation coefficient (r) of 0.988 showing a high correlation of the results obtained by all methods.

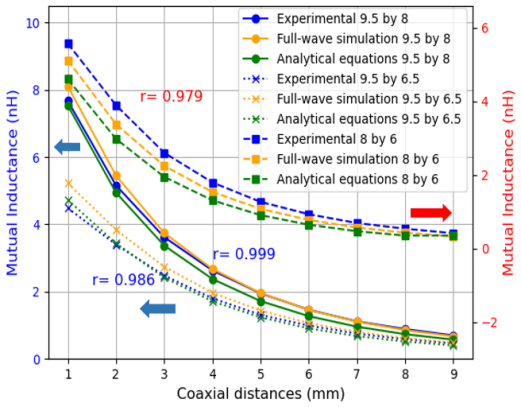

Fig. 6: Evolution of *M* for loops of diameters 9.5, 8 and 6 mm with variation of coaxial distance between their centres, for experimental, simulation and coding methods.

In Fig. 7, two parallel axis cases are presented. Here, the distance between the centers of the loop vertically is 3 and 5 mm, while the horizontal distance is varied. The RMSE of the green plot (Z = 5mm) in Fig. 7 is 0.06 and 0.016 for experimental and analytical results respectively, taking the simulated results as reference. For the red plot, these values are 0.125 and 0.275 respectively. The *M* obtained by experimental means is slightly different because the actual geometry is not perfectly circular. Overall, the results are highly correlated and hence results obtained by our code can be used to simulate loop coupling whatever their positions and orientations.

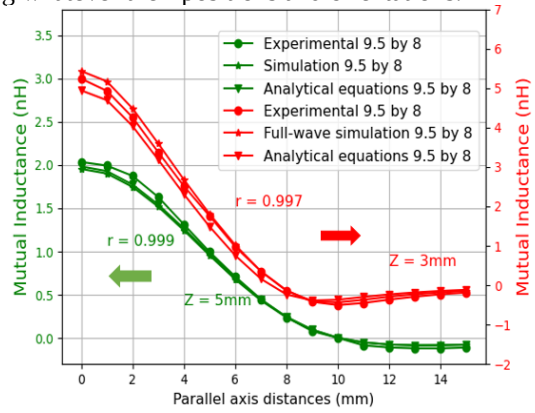

Fig. 7: Evolution of *M* at a constant vertical distance of 3 and 5 mm between their centres with variation parallel axis distances

IV. Validation of Extraction of Equivalent Coupling Surface using NFS

A. *Validation case 1: loop mounted on a PCB*

In this section, the method presented in Section II is implemented. In order to test the approach, a circular loop of diameter 6.5 mm is mounted on a FR4 two-layer PCB (Fig. 8). Using a through-hole connection, the loop is connected to an SMA on the other side of the PCB. Calibration is done up to

this point and then it is connected to VNA. Another H-probe of diameter 6.5 mm, connected to the NFS robot, is moved at different positions and orientations close to the loop on the PCB and the values of *M* is evaluated.

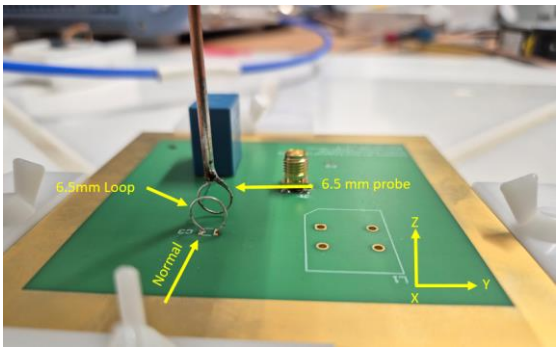

Fig. 8: Coupling between a 6.5 mm loop mounted on an FR4 two-layer PCB and a mobile 6.5 mm connected to the NFS robot.

As it can be seen in Figs. 9 and 10, the experimental and computed values of *M* are in excellent agreement. This proves that it is possible to couple a probe onto a component on the PCB and accurately extract *M*.

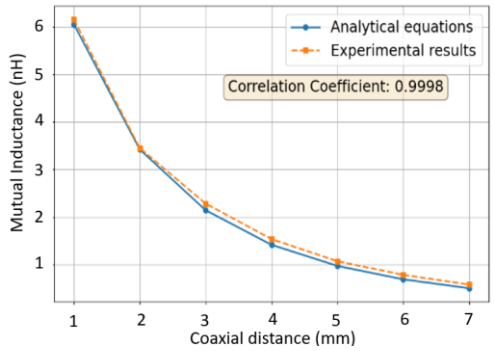

Fig. 9: Plot of M for coaxial arrangement between a circular 6.5 mm loop mounted on a FR4 two-layer PCB and a 6.5 mm circular H-probe.

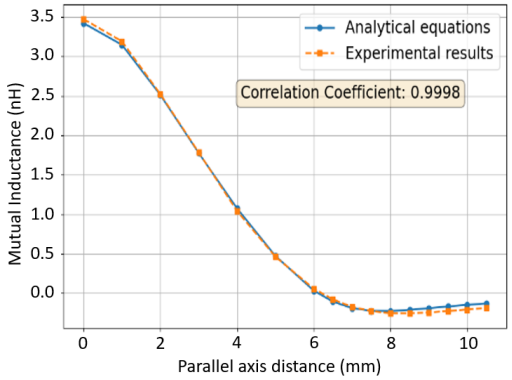

Fig. 10: Plot of *M* for parallel axis arrangement between a circular 6.5 mm loop mounted on a FR4 two-layer PCB and a 6.5 mm circular H-probe with a separation distance of 2mm between their centres.

B. Validation case 2: coupling with a film capacitor

Having proven this, the loop on the PCB is replaced by a capacitor. A 0.33 µF film capacitor (EPCOS 871-B32922D3334K) of packaging 18 mm by 8.5 mm by 14.5 mm (L x W x H) is mounted on one side of the PCB (Fig. 11). On the opposite side of the PCB, an SMA connector is connected to the pins of the capacitor using a very short trace. The same H-field probe is the used to scan at specific distances around the component. The orientation of the probe is changed for each scan. The value of *M* is then obtained using (5). In [9], a TEM cell was used to extract *M* between a probe and the component. However, this method is limited to only extracting *M* at maximum and minimum values, by changing the orientation of the PCB hence change in the field direction. In the presented methodology, it is possible to evaluate *M* at any desired positions using near-field scanning method. A rectangular box of, 27 mm x 18 mm x 15 mm (L x W x H), is defined around the capacitor and the probe is moved along this box. A secure distance of 1 mm is added. In total, the center of the probe is 4.25 mm from the body of the capacitor. The value of *M* is then computed at these points and the field map of *M* distribution around the component is presented below. In the first case, the probe is oriented such that its normal is along the x- axis, where it aligns with the length of the capacitor This is as seen in Fig. 11.

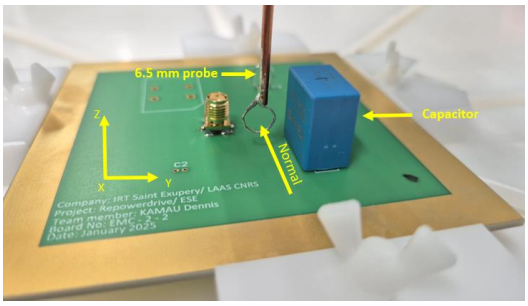

Fig. 11: A 6.5 mm H-probe whose normal is oriented along x-axis scanning at a defined box volume around a 27 mm x 18 mm x 15 mm capacitor

A plot of evolution of *M* in this orientation and along L of capacitor is presented in Fig. 12. A maximum value 0.254 nH of *M* is recorded when the probe center is located at 4 mm above the PCB and a distance of approximately 22 mm (L). A minimum value of 40 pH is recorded at a distance 4.25 mm from the body of the capacitor. This value is as expected to be low, as the probe and the ECS loop are oriented perpendicular to each other. The first inset shows the *M* distribution in the top plan while the second one corresponds to this plan along L of the capacitor, with this probe orientation, Fig 11.

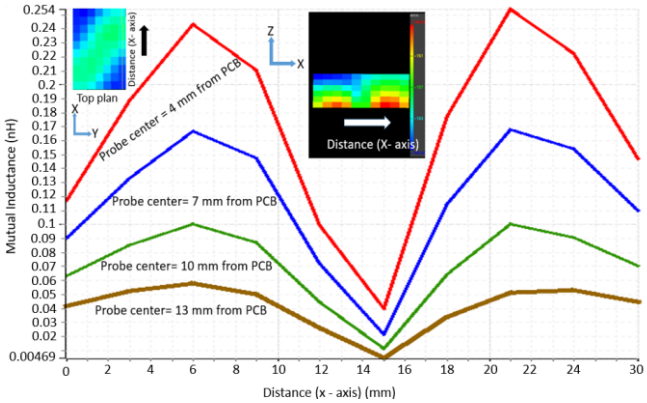

Fig. 12: A plot of evolution of M along L of a capacitor with a probe of 6.5 mm whose normal oriented along x-axis as shown in fig 11. In the inset is a field map.

The orientation of the probe is then changed and the normal of the probe was aligned along the y axis as shown in Fig. 13.

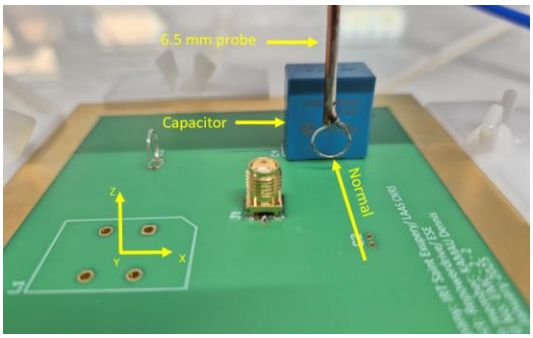

Fig. 13: A 6.5 mm H-probe whose normal is oriented along y-axis scanning at a defined box volume around a 27 mm x 18 mm x 15 mm capacitor

Similarly, a plot of evolution of *M* along the X axis (L of capacitor) is presented in Fig. 14. The frequency value considered in this case was 80.3 MHz. A maximum value 0.359 nH of *M* is recorded when the probe is located at 4 mm above the PCB and a distance of approximately 13 mm (L) which corresponds to the center of ECS of the capacitor. The first inset shows the *M* distribution in the top plan while the second one corresponds to this plan along L of the capacitor, with this probe orientation, Fig 13. From the results in Figs. 12 and 14, it can be seen that the ECS is approximately oriented along the pins of the capacitor. The authors in [9], conclude that the equivalent loop of the capacitor can be approximated to be located exactly where the pins of the capacitor are located. However, as it can be observed in the field map in Fig. 12, it can be seen that there is some asymmetry in the orientation of the equivalent loop. This is further confirmed by the difference in the values of *M* at the same offset distance from the center of the capacitor in Fig. 12, i.e. at distance 5 mm, *M* = 0.22 nH and at distance 22 mm, M = 0.254 nH. These values should be supposedly equal, but the exhibit 15 % difference. The ECS exhibits a slight inclination, something that the authors in [9] might have not investigated due to the limitations of using a TEM cell.

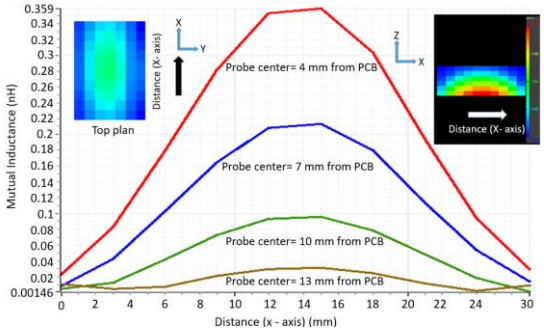

Fig. 14: A plot of evolution of M along L of a capacitor with a probe of 6.5 mm whose normal oriented along y-axis as shown in fig 13. In the inset are the field map.

In this section, we have proven that it is possible to extract *M* of a loop and of a component using NFS. We also have tried to extract the ECS of the capacitor manually. In the following section, we will validate GEMSEO optimization tools [12] that will help us to extract the ECS with more precision and automatically.

V. VALIDATION OF GEMSEO OPTIMIZATION TOOLS

A. Validation using the 6.5 mm diameter loop

In this sub-section, the GEMSEO tools are validated by testing the recovery of loop parameters that are known by a priori. The fixed loop on the PCB set up shown in Fig. 8 is reused. An experimental set up is made where a box is defined around the fixed loop. The fixed loop has the following parameters; Radius (R_P) = 3.75 mm, Center (X_P, Y_P, Z_P) = (0, 0, 3.75 mm) and Theta (θ) = 90° The NFS H- probe is used to scan around this fixed loop following the path defined by the box of 6mm x 8.5mm x 9mm. The fixed loop is located at the center of this box and its center at 3.75 mm above the PCB. The values of transfer impedance at each of these positions are the captured using the VNA. The values of *M* are then computed by post processing. This procedure is then repeated for different orientations of the H-probe i.e. changing theta of the moving H-probe. A dataset is then created and the GEMSEO optimization process described in Fig. 3 is used to recover the parameters of the fixed loop. The table below presents the GEMSEO optimization results. Here, a 200-point LHS of the 5-D parameter space is chosen.

Table 1: GEMSEO optimization results versus true values

Parameters	**True Values**	**Optimization (GEMSEO)**
Radius (R_P) (mm)	3.75	3.975 (Δ = + 6 %)
Center (X_P) (mm)	0	-0.000018 (Δ = – 0.018 µm)
Center (Y_P) (mm)	0	0.00516 (Δ = + 5.16 µm)
Center (Z_P) (mm)	3.75	3.88 (Δ = + 3.5 %)
Theta (θ) (°)	90°	89.96° (Δ = – 0.044 %)

The whole optimization process consumes 3 minutes. From the table above, it can be seen that GEMSEO extracts the location an orientation of the fixed loop with high accuracy hence validating the optimization approach.

B. GEMSEO robustness to noise

It is essential to ensure that the optimization is robust to noise. To test this, a dataset of two circular loops is initially created by coding i.e. parameters of the primary loop: Radius (R_P) = 2 mm, Center (X_P, Y_P, Z_P) = (2.5, 2.5, 2.5) and Theta (θ_P) = 20°. A secondary loop of radius 3 mm assumed to scan around the fixed loop making a box of 7mm x 7mm x 7mm. The values of *M* are then generated using the code based on (4). First, the values of the fixed loop are recovered using GEMSEO before noise injection. Secondly, three types of noise are then injected i.e. a zero-mean normal noise with a standard deviation of 2% of the intrinsic spread of M, simulating random measurement fluctuations that cluster around the correct value, such as thermal noise and equipment jitter. A global bias of (+3%), by multiplying each *M* with 1.03. This represents errors such as offsets in sensor calibration and extra geometric scaling factors. Lastly, mixed noise with outliers was added to *M* values. In this case, a little amount of modest Gaussian noise (σ = 1 %) is added and then five random samples are chosen to receive a ±10% "spike" in order to simulate sporadic large deviations. This represents noise from probe misplacement or transitory interaction with surrounding objects. The table below summarizes the recovered values before noise and after noise

injection. The value in brackets represents the percentage deviation from the true value.

Table 2: Analysis of noise impact on GEMSEO optimization tools

Noise	R_P (%)	center_ X_P (%)	center_ Y_P (%)	center _ Z_P (%)	θ (%)
Before noise	2.09 (+5)	2.55 (+2)	2.44 (–2)	2.52 (+1)	17.45° (–13)
Gaussian σ ≈ 2 %	2.11 (+5.2)	2.55 (+2)	2.45 (– 2.3)	2.53 (+1.0)	17.32° (– 13)
Global bias +3 %	2.21 (+6.1)	2.49 (+1.5)	2.37 (– 3.3)	2.51 (+0.7)	18.713 (– 11)
Mixed (+ 5 outliers ±10 %)	2.098 (+4.9)	2.547 (+1.9)	2.44 (– 2.4)	2.52 (+0.9)	17.47 (– 12.6)

All four geometric coordinates are recovered to within ± 2–5%. In most cases, in non-linear inverse problems, the inverse mapping frequently amplifies the input noise. Theta (θ) is seen to have the same deviation of (13%) before and after noise injection. This can be explained using the notion that it primarily modifies the relative orientation of the two loops, a second-order influence on the Neumann integral, hence it is naturally less visible than the translational parameters. Also, the angular resolution is limited by ten segments per loop; the parameter primarily impacted by discretization error is θ. However, this appears to be a decent trade-off because as adding more segments results in a longer optimization duration. Since this model depends on the parameters non-linearly, the noise which is introduced at the beginning as 2% in *M*, becomes about a 5% uncertainty in the recovered geometry for the Gaussian case. For the global bias case, although the optimizer seems to follow the direction of the systematic scale rather than correcting it, the model is still able to recover the values with high accuracy. Doing a separate calibration measurement to remove the bias is essential. For the mixed case, the gross errors are down-weighted and the recovered parameters are very close to the true values. This shows that the optimization model shields the solution against a minimal number of spurious points, allowing the full data set to be kept instead of having to manually removing "bad" records. In all the noise analysis, θ is confirmed to be the most sensitive to measurement noise. It can be seen that a random instrumentation noise of a few percent will not compromise ECS extraction. It can hence be concluded from these noise analyses that the optimization approach used is highly robust and can withstand different kinds of noise.

VI. Conclusion

There is a need to develop a contactless and in-situ method to characterize the EMI filter in its real operating conditions. The proposed method relies on coupling between a magnetic NFS probe and a component of the filter and the extraction of the ECS of the component. The NFS probe is preferred because it provides more information on the ECS compared to the TEM cell (e.g. to detect the tilt of the surface within the component) which is important in accurate extraction of *M* and evaluating parasitic coupling. In the work presented above, an approach to extract the ECS of a EMI filter component using the magnetic NFS probe is presented. For robustness, an analytical formulation of *M* is presented and validated which is then used for the extraction of the ECS. A non-linear optimization process using GEMSEO is used to recover the ECS parameters of a loop on a PCB, which are known by a priori, and its robustness to noise is validated. As such, we propose to reuse this optimization process to recover the unknown ECS parameters of an EMI filter component. Future works will focus on more complex components such as common-mode chokes.

Acknowledgment

We would like to thank RePOWERDRIVE team at IRT Saint Exupéry - Toulouse for provision of the optimization tools and excellent EMI analysis facilities at IRT Saint Exupéry. Many thanks to LAAS CNRS for helping in the fabrication of the PCB used in this study.

These results have been obtained in the framework of the IRT Saint Exupéry's research projects RePOWERDRIVE. We acknowledge the financial and in-kind support (background knowledge and services) from the IRT Saint Exupéry's, industrials and academic members and the financial support of the French National Research Agency.

References

[1] CISPR17: Methods of measurement of the suppression characteristics of passive EMC filtering devices, International Electrotechnical Commission (IEC) Std.

[2] "IEEE Standard for Methods of Measurement of Radio Frequency Power Line Interference Filter in the Range of 100 Hz to 10 GHz," in IEEE Std 1560-2005, vol., no., pp.1-92, 24 Feb. 2006.

[3] T. Dörlemann, S. Frei, R. Perraud, S. Serpaud, F. Kapaun and D. Guedon, "Parallel-Cascaded Narrow-Band Adaptive Digital Active EMI Filters for Broadband CM-Noise Reduction in Motor Inverters," in *IEEE Transactions on EMC*, vol. 66, no. 5, pp. 1440-1449, Oct. 2024.

[4] A. Boyer, S. Ben Dhia and S. Serpaud, "In-Situ and Contactless Evaluation of Performance of Power Converter EMC Filter based on Near-Field Scan Measurement," 2023 International Symposium on Electromagnetic Compatibility – EMC Europe, Krakow, Poland, 2023.

[5] H. Weng, D. G. Beetner, R. E. DuBroff, J. Shi, "Estimation of High-Frequency Currents From Near-Field Scan Measurements", IEEE Trans. on EMC, vol. 49, no. 4, Nov. 2007.

[6] X. Dong, S. Deng, D. G. Beetner, T. H. Hubing, and T. P. Van Doren, "Determination of high frequency package currents from near-field scan data," in Proc. IEEE Symp. EMC., Aug. 8–12, 2005, pp. 679–683.

[7] A.D.Yaghjian, "An overviewof near-field antenna measurements," IEEE Trans. Antennas Propag., vol. AP-34, no. 1, pp. 30–45, Jan. 1986.

[8] S. Serpaud, "Application de la méthode de mesure champ proche en émission pour l'aide à la conception et à l'investigation des non-conformités CEM des cartes électroniques", Ph.D. dissertation, INSA Toulouse, Univ. of Toulouse, Toulouse, France, 2023.

[9] M. Stojanovic, F. Lafon, S. Op't Land, R. Perdriau and M. Ramdani, "Determination of Equivalent Coupling Surface of Passive Components Using the TEM Cell," in IEEE Transactions on EMC, vol. 60, no. 2, pp. 298-309, April 2018

[10] D. Wanyoike, A. Boyer, S. Serpaud, "In-Situ and Contactless Extraction of the Insertion Loss of Switched Mode Power Supply EMC Filter based on Near-Field Scan Measurement", Workshop Electromagnetic Compatibility, ESEO, Angers, GDR Ondes 2024.

[11] S. Babic, F. Sirois, C. Akyel and C. Girardi, "Mutual Inductance Calculation Between Circular Filaments Arbitrarily Positioned in Space: Alternative to Grover's Formula," in IEEE Transactions on Magnetics, vol. 46, no. 9, pp. 3591-3600, Sept. 2010.

[12] https://gemseo.readthedocs.io/en/stable/examples/optimization_problem/plot_simple_opt_2.html#sphx-glr-examples-optimization-problem-plot-simple-opt-2-py